Journal of Population Therapeutics & Clinical Pharmacology

RESEARCH ARTICLE
DOI: 10.47750/jptcp.2023.30.12.008

Fractional Diffusion Equation for Medical Image Denoising using ADI Scheme

A. Abirami[1]* , P.Prakash[2]
[1]Department of Mathematics, Sona College of Technology, Salem 636 005, India
[2]Department of Mathematics, Periyar University, Salem 636 011, India.
***Corresponding author:** A.Abirami , Department of Mathematics, Sona College of Technology, Salem 636 005, India, Email: mentor.abhi@gmail.com

Submitted: 10 March 2023; Accepted: 12 April 2023; Published: 08 May 2023

ABSTRACT
This paper proposes a fractional order total vari- ation model for additive noise removal which uses a different fractional order of the regularization term of the objective function. The denoising model based on space and time fractional derivatives on a finite domain is discretized with effective applications of Gru¨nwald-Letnikov(G-L) and Caputo derivatives. This model has been adopted to solve Alternative Direction Implicit (ADI) scheme to denoise medical images. The advantage of this model is for smooths the homogeneous regions and enhance edge information revealing more details of the image. The results show that the proposed model has desirable feedback for enhancing medical images, revealing more detailed information than ROF(Rudin, Osher and Fatemi), TV − L1 (Total Variation L1 space) and fourth order partial differential equation based models.

Keywords: *fractional order total variation; Grunwald Letnikov; Caputo derivative; ADI scheme; medical image denoising*

INTRODUCTION
The fractional calculus has become an important branch of mathematical analysis in signal and image processing. Many algorithms and models based on fractional calculus for achieving enhancement have been developed. TV [17] is the most commonly used method due to its simplicity and comparatively better performance on almost all types of images. This successful variational model is proposed by Rudin, Osher and Fatemi(ROF). However, both from theoretical and experimental points of view, the TV model suffers from staircase effect. In [9,21,22] the authors have established a second order partial differential equation based image denoising model. In [10,12,24,26] the fourth order partial differential equation based denoising models proved to be effective in solving staircase effect problem.

The fractional order derivative models under the variational framework have been presented in several previous works [2,3,4,5,15,16,18,23,27]. Matheieu et al. [13] introduced edge detector based on fractional differentiation. The modified TV-ROF image denoising model based on Split Bregman iterations introduced in [7]. Zhang et al. [26] studied the spatial telegraph equation which could be applied to image denoising. Recently, Abirami et al. [1] contributed a new algorithm based on CN-GL scheme for image denoising. The second order partial differential equation uses increasing function regard to gradient operator absolute value as integrand of energy functional.

This partial differential equation can better preserve edges when removing the noise, but the resulting image may contain serious blocky effect. Fourth order partial differential equation model uses increasing function regard to Laplacian operator absolute value as integrand of energy functional. The resulting image's smoothness is better than second-order partial differential equation because Laplacian operator cannot determine edges. The fourth order partial differential equation model blurs edge information. Therefore, to avoid this type of problem recently several researches have concentrated only on fractional order domain.

In this paper, we present a new approach based on fractional derivatives which allows us to handle the total variation. The smoothing in the image terminology is performed by means of a single parameter in a nonlinear fractional partial differential equation. Besides, satisfactory practical results were also obtained by proposed model. The experimental results prove that it can not only preserve the low-frequency contour feature in the smooth area but also the nonlinearity maintained the high frequency edge and texture details in the areas of medical images. The outline of the paper is as follows.

First, it introduces three common used definitions of fractional calculus and review some closely related work on reducing the staircase effect including integer-order and fractional order variation models for image denoising. Second we study fractional order diffusion equation from fractional order total variation model. On the basis, a space and time fractional partial differential equation is proposed. Third, we prove stability and convergence of the model. Finally we show that the denoising capabilities of the proposed model by comparing with ROF model, TV − L1 model, and fourth order denoising models.

RELATED WORK

The commonly used definitions of fractional calculus in the Euclidean measure are Riemann-Liouville and Caputo which are premise of the fractional developmental equation based on the denoising models.

Riemann-Liouville: It's a fractional integral operator and defined as

$$J^{\alpha}u(x,t) = \frac{1}{\Gamma(\alpha)}\int_0^x (x-t)^{\alpha}u(t)dt$$

Caputo-derivative: This fractional derivative operator, Dα of order α is defined as with

$${}^{C}D^{\alpha}u(x,t) = \frac{1}{\Gamma(m-\alpha)}\int_0^x \frac{u^m(t)}{(x-t)^{\alpha-m+1}}dt, \alpha > 0$$

$m-1<\alpha\le m, m\in N, x>0.$

Now we briefly review some related models for image denoising:

Total Variation (TV) model: Total Variation [17] is the most commonly used model due to its openness and similarly better achievement on almost all types of images. This successful variational model is proposed by Rudin, Osher and Fatemi (ROF) and which is expressed as:

$$E(u) = \min_{u\in\Omega}\left\{\int_{\Omega}|\nabla u|dxdy + \frac{\lambda}{2}\int_{\Omega}(u-f)^2dxdy\right\}$$

,

where $|\nabla u| = \sqrt{u_x^2+u_y^2}$ and λ is a positive parameter.

TV − L1 model: The (ROF) model, the TV − L1 model [2,11] is defined as the following variational problem.

$$E(u) = \min_{u\in\Omega}\left\{\int_{\Omega}|\nabla u|dxdy + \frac{\lambda}{2}\int_{\Omega}(u-f)dxdy\right\}$$

,

The difference compared to the (ROF) model is that the squared L2 data fidelity term has been replaced by the L1 norm. Although the change is small, this model offers some desirable properties. The TV −L1 model is more effective than the (ROF) model in removing impulse noise (example salt and pepper noise) [14] and is contrast invariant. Therefore this model has a strong geometrical meaning which makes it useful for scale-driven feature selection and denoising of shapes. Being not strictly convex, computing a minimizer of this model is a hard task.

Fourth order partial differential equation based model: In [24], a fourth order partial differential equation based denoising model has been proposed and proved the effectiveness in solving the staircase effect problem and abilities to avoid the blocky effects widely seen in images processed by anisotropic diffusion, while achieving the degree of noise removal and edge preservation comparable to anisotropic diffusion(second order partial differential equations). The model is expressed as

$$E(u) = \min_{u\in\Omega}\left\{\int_\Omega f\left(|\nabla^2 u|\right)dxdy\right\}$$

where $|\nabla 2u| = \sqrt{u_{xx}^2 + u_{yy}^2}$ and it defines Laplacian operator. However, the fourth order partial differential equation based models suffer from the blurring effect near edges due to the possible over smoothing.

Proposed Space and Time Fractional Order Model

We propose a new fractional variational model based on space and time fractional order derivatives. It is observed that the image edge direction and texture details are important information for the image up-sampling process. Thus, we may need operators that can detect the edge direction to enhance the texture details so that different orders take effect in different regions. Fractional order derivative can meet this need. The fractional order TV model is defined as:

$$\min_{u>0} E(u) = (1-e^{-\lambda})^2\int_\Omega |\nabla^\alpha u| dxdy + \frac{\lambda}{2}\int_\Omega (u-f)^2 dxdy,$$
$$x_L < x < x_R, y_L < y < y_R$$

where $1 < \alpha \leq 2$ refers the preservation of magnitude of low frequency by fractional order differentiation is better than that by second, fourth order differentiation and $\lambda > 0$ is a parameter that adjusts the contribution of the fidelity term and the term $(1 - e{-}\lambda)2$ is strictly used to minimize the value of the energy function in this paper. So the proposed model works very efficiently for denoising the images.

In this model, there are two basic ideas behind the selection of fractional order differentiation. First, fractional order differentiation is not a local property of an image. Second, integer order and fractional order differentiations can enhance high frequency components, but the enhancement of integer order differentiation consequently fractional order differentiation introduces relatively low contrast and avoids very large oscillation near edges. When $\alpha = 0$, the proposed model becomes the TV model and when $\alpha = 2$, the proposed model becomes the second and fourth order variation models.

To implement the proposed model, we need to derive the fractional Euler-Lagrange equation.

$$0 = (1-e^{-\lambda})^2(-1)^\alpha\nabla^\alpha\cdot\left(\frac{\nabla^\alpha u}{|\nabla^\alpha u|}\right) + \lambda(u-f).$$

Using the steepest descent method, we derive the associated heat flow equation (1),

$$\frac{\partial^\beta u}{\partial t^\beta} = (1-e^{-\lambda})^2(-1)^\alpha\nabla^\alpha\left(\frac{\nabla^\alpha u}{|\nabla^\alpha u|}\right) + \lambda(u-f)$$

$$\frac{\partial^\beta u}{\partial t^\beta} = (1-e^{-\lambda})^2(-1)^\alpha\nabla^\alpha\left(\frac{\nabla^\alpha u}{\sqrt{|\nabla^\alpha u|^2+\epsilon}}\right) + \lambda u - \lambda f \quad (1)$$

where $0 < \beta \leq 1$ is the time fractional derivative and ϱ > 0 is introduced to avoid singularity.

The solution procedure uses an equation in terms of time as an evolution parameter. If we choose dt then it's too big and iteration process is not stable. If it's too small then, it consumes time.

The evolution model (2) is initialized with noisy image u(x,y,0) = f(x,y), and homogeneous Neumann boundary conditions [19],

Ui,Nn = Ui,Nn −1;UN,jn = UNn−1,j on ∂**Ω** (2)

where i = 0,1,2...M, j = 0,1,2...N.

Let unij be the approximation to the value u(xi,yj,tn) where xi = iΔx, yj = jΔy and tn = nΔt, n ≥ 1. We discrete the equation (2) by Gr¨unwald-Letnikov and Caputo fractional derivatives.

The spatial fractional derivatives with right shifted G-L formula is employed at level tn with respect to the variables x and y respectively.

$$\nabla_x^\alpha u_{i,j}^n = \frac{1}{(\Delta x)^\alpha}\sum_{k=0}^{i+1} g_k^{(\alpha)} u_{i-k+1,j}^n;$$

$$\nabla_y^\alpha u_{i,j}^n = \frac{1}{(\Delta y)^\alpha}\sum_{k=0}^{j+1} g_k^{(\alpha)} u_{i,j-k+1}^n.$$

Let $\overline{\nabla}_x^\alpha$ and $\overline{\nabla}_y^\alpha$ be the adjoint operators of ∇αx and ∇αy respectively, and defined by

$$\overline{\nabla}_x^\alpha u_{i,j}^n = \frac{1}{(\Delta x)^\alpha}\sum_{k=0}^{i+1} g_k^{(\alpha)} u_{i+k+1,j}^n;$$

$$\overline{\nabla}_y^\alpha u_{i,j}^n = \frac{1}{(\Delta y)^\alpha}\sum_{k=0}^{j+1} g_k^{(\alpha)} u_{i,j+k+1}^n,$$

Also the normalised Gr¨unwald weights are stated by

$$g_k^{(\alpha)} = \frac{(-1)^k\alpha(\alpha-1).(\alpha-2)\cdots(\alpha-k+1)}{k!}$$

and remark that these normalized weights depend only on the order α and the index k. The first four terms of this sequence are given by

$$g_0^\alpha = 1, g_1^\alpha = -\alpha, g_2^\alpha = \frac{\alpha(\alpha-1)}{2!}, g_3^\alpha = \frac{-\alpha(\alpha-1)(\alpha-2)}{3!},\cdots.$$

The fractional order time derivative will be replaced by Caputo fractional derivatives of the 3rd order approximation,

$$\frac{\partial^\beta u_{ij}^n}{\partial t^\beta} \cong \frac{\tau^{-\beta}}{\Gamma(2-\beta)}\sum_{s=0}^{n} b_s(u_{ij}^{n+1-s} - u_{ij}^{n-s}),$$

where bs = (1 + s)1−β − s1−β and s = 0,1,2...n;n ≥ 1 and we consider

$$\frac{L_{\alpha,t}u_{ij}^n}{\tau^{-\beta}} = \frac{1}{\Gamma(2-\beta)}\sum_{s=0}^{n} b_s(u_{ij}^{n+1-s} - u_{ij}^{n-s}). \quad (3)$$

Denote the time step by τ, the discrete version of the equation (2) is represented by

$$\frac{\tau^{-\beta}}{\Gamma(2-\beta)}\sum_{s=0}^{n} b_s(u_{ij}^{n+1-s} - u_{ij}^{n-s}) = (1-e^{-\lambda})^2(-1)^\alpha\left\{\overline{\nabla}_x^\alpha\left(\frac{\nabla_x^\alpha u_{ij}^n}{\sqrt{(\nabla_x^\alpha u_{ij}^n)^2+(\nabla_y^\alpha u_{ij}^n)^2+\epsilon}}\right)+\overline{\nabla}_y^\alpha\left(\frac{\nabla_y^\alpha u_{ij}^n}{\sqrt{(\nabla_x^\alpha u_{ij}^n)^2+(\nabla_y^\alpha u_{ij}^n)^2+\epsilon}}\right)\right\}+\lambda u_{ij}^n-\lambda f_{ij}^n$$

. where we consider a1 = Γ(2 − β)(−1)α(1 − e−λ)2 and $a_2 = \frac{\Gamma(2-\beta)}{\tau^{-\beta}}\lambda$.

The finite difference operations are described as follows:

$$L_{\alpha,x}u_{ij}^n + L_{\alpha,y}u_{ij}^n = \frac{(-1)^\alpha}{\tau^{-\beta}}\left\{\overline{\nabla}_x^\alpha\left(\frac{\nabla_x^\alpha u_{ij}^n}{\sqrt{(\nabla_x^\alpha u_{ij}^n)^2+(\nabla_y^\alpha u_{ij}^n)^2+\epsilon}}\right)+\overline{\nabla}_y^\alpha\left(\frac{\nabla_y^\alpha u_{ij}^n}{\sqrt{(\nabla_x^\alpha u_{ij}^n)^2+(\nabla_y^\alpha u_{ij}^n)^2+\epsilon}}\right)\right\}. \quad (4)$$

$$u_{ij}^{n+1} - u_{ij}^n + L_{\alpha,t}u_{ij}^n = a_1(L_{\alpha,x}u_{ij}^{n+1} + L_{\alpha,y}u_{ij}^{n+1}) + a_2(u_{ij}^n - f_{ij}^n),$$

(1 − a1Lα,x − a1Lα,y)unij+1 = (1 − Lα,t + a2)unij − a2fijn, (5)

The most suitable method in solving classical multi-dimensional diffusion equations is ADI scheme and it is used to significantly reduce the computational cost. The ADI scheme has been used to solve the two-dimensional space fractional diffusion equation [1]. For using ADI scheme, some perturbations of equation (6) used to derive schemes that are specified and solved in one direction at a time, and for this problem the equation (6) is written in a separate form

$$(1-a_1L_{\alpha,x})(1-a_1L_{\alpha,y})u_{ij}^{n+1} = (1-L_{\alpha,t}+a_2)u_{ij}^n - a_2f_{ij}^n, \quad (6)$$

which produces an additional perturbation error as follows:

$$\tau^{-2\beta}(L_{\alpha,x}L_{\alpha,y})u_{ij}^{n+1}.$$

Equation (7) can be divided into two equations, using an intermediate solution u∗i,j,

(1 − a1Lα,x)u∗i,j = (1 − Lα,t + a2)uijn − a2fijn, (7)

$$(1-a_1L_{\alpha,y})u_{i,j}^{n+1} = u_{i,j}^*. \quad (8)$$

The intermediate solution u∗i,j in equations (8) and (9) is defined to advance the numerical solutions unij at time tn and $u_{i,j}^{n+1}$ at time tn+1. Here, the ADI scheme is worked in two different ways. First, a set of Nx − 1 equations in x-direction (for each fixed yj)are solved to obtain the intermediate solution u∗i,j from equation (8) and second to change the spatial direction, a set of Ny − 1 equations in y-direction (for each fixed xi) are solved to obtain the solution $u_{i,j}^{n+1}$ by using the intermediate solution u∗i,j from the first step. If $\alpha \in (1,2]$ and $\beta \in (0,1]$, then the equation (1) is unique, unconditionally stable, consistent and its temporal partial derivative up to order α+1 and spatial partial derivatives up to order r, where r > α + β + 3. The ADI scheme is defined by (6) for solving (1) also from [17] proved the truncation error (in Table 2) of the form O(Δx) + O(Δy) + O(Δt) and (Lα,xLα,yunij+1) converges to mixed partial derivative of order O(Δx)+O(Δy). Hence the numerical solution of u_{ij}^{n+1} and unij are calculated from the initial and boundary conditions (3).

As a result, the discrete algorithm for solving the proposed model is summarized as follows:

Initialization: fix u0 = f,α = 1.6,β = 0.5,τ = 0.05.

Update u_{ij}^{n+1} by (9).

Check if $\frac{||u_{ij}^{n+1} - u_{ij}^{n}||}{||u_{ij}^{n}||} \leq$ total; then stop.

Set unij+1 = u(x,y).

Output display u(x,y).

Stability Analysis

In this section, we have considered the stability analysis of the implicit finite difference approximation equation (8).

Theorem 4.1. Each one dimensional implicit system defined by the linear difference equations (8) and (9) is unconditoionally stable for all 1 < α ≤ 2 and 0 < β ≤ 1.

Proof. At each grid point yk for k = 1,...,Ny − 1, consider the linear system of equation defined by equation (8). This system of equations may be written as AkUk∗ = (1 − Lα,t + a2)Ukn + Fkn, where incorporating the boundary conditions from equation (9). We have

$$U_k^* = [u_{1,k}^*, u_{2,k}^*, ..., u_{N_x-1,k}^*]^T,$$

(1 − Lα,t + a2)Ukn + Fkn = [(1 − Lα,t + a2)U1n,k−,a2f1n,k(1 − Lα,t + a2)U2n,k − a2f2n,k,..., (1 − Lα,t + a2)UNnx−1,k − a2fNnx−1,k]T

and Ak = [Aij] is the Nx − 1 × Nx − 1 matrix of coefficiets resulting from the system of difference equations at the gridpoint yk, where the matrix entries along the ith row are defined from equation (8). For i = 1 the equation becomes

$$-D_{1,k}L_{\alpha,2}U_{0,k}^* + (1 - D_{1,k}L_{\alpha,1})U_{1,k}^* - D_{1,k}L_{\alpha,2}U_{2,k}^* = (1 - L_{\alpha,t} + a_2)U_{1,k}^n + a_2 f_{1,k}^n$$

,

For i = 2 the equation becomes

$$-D_{2,k}L_{\alpha,3}U_{0,k}^* - D_{2,k}L_{\alpha,2}U_{1,k}^* + (1 - D_{2,k}L_{\alpha,1})U_{2,k}^* - D_{2,k}L_{\alpha,0}U_{3,k}^* = (1 - L_{\alpha,t} + a_2)U_{2,k}^n + a_2 f_{2,k}^n$$

,

For i = Nx − 1 the equation becomes

−DNx−1,kLα,NU0∗,k − DNx−1,kLα,Nx−1U1∗,k + ... + (1 − DNx−1,kLα,1)UN∗x−1,k − DNx−1,kLα,0UN,k∗

= (1 − Lα,t + a2)UNnx−1,k + a2fNn+1x−1,k.

where the coefficients $D_{i,k} = \frac{a_1 \tau^\beta}{\Delta x \alpha}$. The entries of the matrix Aij for i = 1,2,...,Nx −1

and Aij for j = 1,2,...,Nx − 1 are defined by Aij =

$-D_{i,k}L_{\alpha,i-j+1}$, where j ≤ i − 1

0

1 − Di,kLα,1, where j=i+1

−Di,kLα,0, where j > i + 1

We will now apply the Grehgorin theorem [11] to conclude that every eigenvalue of the matrix Ak has a magnitude strictly larger than 1. According to the theorem, every eigen value λ of the matrix Ak has a real part larger than one. This proves that the method is stable. When sweeping in the alternate diection to solve for un+1 from u∗,then the Similar results hold for the finite difference equations defined by (10). Hence this system is unconditionally stable.

Covergence Analysis

The Table 2 shows the order of the convergence of the model as the grid is refined as all step sizes are halved. The ADI scheme is defined by (6) for solving (1) also from [17] proved the truncation error (in Table 1) of the form O(Δx)+O(Δy)+O(Δt) and (Lα,xLα,yunij+1) converges to mixed partial derivative of order O(Δx) + O(Δy).

Experimental Results

Medical image denoising is a more significant method which leads physicians in investigation of diseases. Medical images from MRI(Magnetic Resonance Imaging), CT(Computed Tomography), PET(Positron Emission Tomography), OCT(Optical Coherence Tomography), X-Ray and Ultrasound etc. These imaging modalities help in the evaluation of various organs of the body like brain, lung, breast, stomach, soft tissues, bone, eyes, teeth and blood vessels. Therefore, removal of noise from medical images is very essential for clinical purposes.

In this section, we test the performance of the proposed model and also compare the results with ROF, TV − L1 [17] and fourth order partial differential equation based models [12,24] in terms of vision and quantitative analysis including the Peak Signal to Noise Ratio(PSNR) and Mean Square Error(MSE) of the restored image which are given by

$$MSE = \frac{1}{MN}\sum_{i=1}^{M}\sum_{j=1}^{N}\left[f(i,j)-u(i,j)\right]^2,$$

$$PSNR = 10*\log_{10}\left(max(f,u)^2 * MSE\right),$$

where f,u and M×N are the restored image, the true image and size of the image respectively. We use five types of medical images as benchmark images as shown in Figures(1-5). Some parameters are chosen as fixed values σ = 10,15,20 and 25 including $\beta = 0.5$ and $\alpha = 1.6$. The proposed model denoises the noised image with the regularization parameter λ chosen in such a way that $0 \le \lambda \le 1$ as suggested in global image threshold using Otsu's method. When λ increases, the smoothing effect increases with size of the neighboring window [1,2]. For $1 < \alpha < 2$, fractional derivative can preserve the low frequency contour feature in the smooth areas and nonlinearly keep high frequency marginal feature in areas where gray level change greatly, and also enhance the texture information in those areas where gray level does not change evidently. For $0 < \beta < 1$, time fractional derivative can preserve stability of the iteration process and reduce computation time. The stopping criterion for the iteration is $\frac{||u_{ij}^{n+1}-u_{ij}^{n}||}{||u_{ij}^{n}||} \ge \epsilon$. We considered ϙ = 10−5 in the numerical experiment. MATLAB 22.0.0. is used in experimental and numerical analysis.

The first experiment is to perform the proposed scheme on the MRI of the cervical spine image (Figure 1(a)). Cervical spine (neck) is soft-housing the spinal cord that communicates informations from brain to control all aspects of the body. This MRI image showed an oblong expansile intramedullary lesion at the c2/c2 level of spinal cord. The noisy image with Gaussian noise is shown in Figure 1(b). The denoising results are shown in Figure 1(c), Figure 1(d), Figure 1(e) and Figure 1(f) respectively. It is observed that the reconstructed denoised images by ROF based model is effective in preserving the ringing artifacts, but it yields piecewise constant block artifacts as shown in Figure 1(c), Figure 1(d) and Figure 1(e). Besides, the ROF model and TV − L1 based models may generate a false grey edge along the spinal cord. The denoising results of proposed model (Figure 1(f)) is the best, which preserves structure and all the information without any loss.

Second experiment is to perform the proposed scheme on the PET/CT of lung image (Figure 2(a)). In this image the lung is affected by cancer. This image has two partition such as CT scan of chest and corresponding PET/CT image showing a mass in the left lung (top arrow). The noisy image Figure 2(b) is affected with Gaussian noise levels σ = 10,15,20 and 25 on CT image. From a subjective view of the visual effect, we know the following from Figure 2(a). First, the denoising capabilities of TV − L1 is worse than the other models, because they obviously diffuse and smooth the high frequency edge and texture details from Figure 2(d). Figure 2(d) and Figure 2(e) have preserved that the texture details are blurred. The denoising capabilities of proposed model (Figure 2(f)) is the best, which preserves the high frequency edge and texture details comparitively other methods.

Third experiment is to perform the proposed scheme on the OCT of retina image (Figure 3(a)). One of the leading causes of blindness is diabetic retinal eye disease which is called as diabetic retinopathy. Figure 3(a) shows the tiny red spots that may lead to haemorrhage. The noisy images

Figure 3(b) are corrupted by different Gaussian levels $\sigma = 10,15,20$ and 25. We list the portion of the up-sampling results by the proposed model and ROF, TV −L1 and fourth order partial differential equation models in Figures 3(c), 3(d) and 3(e). From the viewpoint of visual effect, we know the following from Figure 3(f) when noise is very strong.

Fourth experiment is to work the proposed scheme on the X-ray image (Figure 4(a)). X-rays makeup type of electromagnetic radiation. This X-ray images were taken during health assessment and had proved to be a useful diagonstic tool that also help to minimize time under anaesthesia. Figure 4(b) is corrupted by Gaussian noise at four different level such as $\sigma = 10,15,20$ and 25. In Figures 4(c), 4(d) and 4(e), structure is not preserved as well as have lost the information. Figure 4(f) provides original information without any loss and can be used for clinical purpose.

Fifth experiment is to perform the proposed scheme on ultra sound liver tumor segmentation image (Figure 5(a)). This ultrasound image is safe and painless and produces pictures of inside the body using sound waves. The noisy image Figure 5(b) is corrupted by different Gaussian levels $\sigma = 10,15,20$ and 25. We list the portion of the up-sampling results by the proposed model and ROF, TV − L1 and fourth order partial differential equation models in Figures 5(c), 5(d) and 5(e). First, the denoising capabilities of TV −L1 is worse than the other models. We can see indistinctly that the contour and the texture details of inner organ can hardly be recognized from Figures 5(c), 5(d) and 5(e). Finally, the denoising capabilities of proposed model is the best because from Figures 5(f). We see that the contour is clear and edge and texture details can be identified.

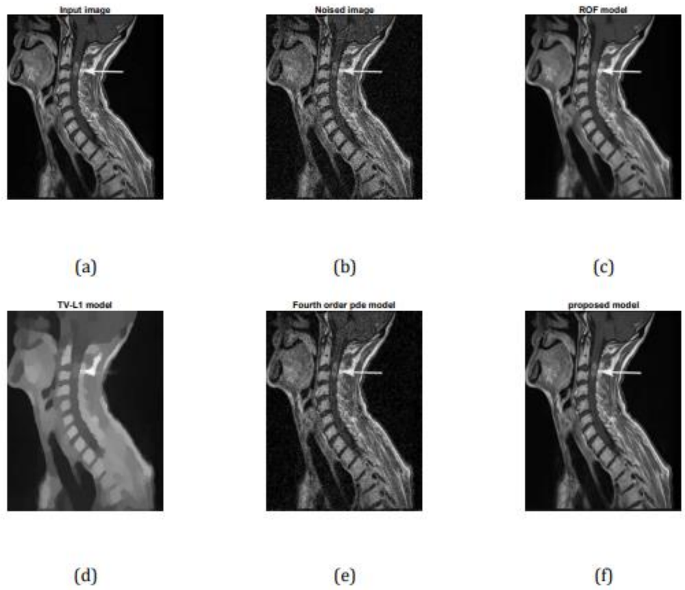

FIGURE 1: The denoising results of MRI-cervical spine image.

Finally, the calculated values and CPU time for all the experiments are shown in Table 2. The comparision of PSNR and MSE value between four models are shown in Figures (6) and (7). In Figure (8), the α values are shown in x−axis and PSNR values obtained from four model are marked in y−axis. It is clearly proved that highest PSNR value is achieved at highest α value and lowest PSNR value is achieved at lowest α value. Most of the real time and online applications require the scheme with less execution time.

CONCLUSION

In this paper, we proposed a variational model on the fractional order derivative. By adaptively combining space and time fractional order in different medical image regions, we proposed a model that can preserve important structures such as degrees and textures and also reduced staircase effect when removing noise. The experimental results confirm the effectiveness of the proposed approach for medical image denoising.

REFERENCES

1. Abirami, P. Prakash and K. Thangavel, Fractional diffusion equation based image denoising using CN-GL scheme,International Journal of Computer Mathematics 95 (2018), 1222–1239.
2. Abirami, A new fractional order total variational model for multiplicative noise removal, Journal of Applied Science and Computations, 6(3) (2019), pp. 483–491.
3. Abirami and P. Prakash Survey on incorporating fractional derivatives in image denoising, Advances in Mathematics:Scientific Journal, 9(3) (2020), pp. 1367–1377.
4. Abirami P. Prakash and Y.K. Ma, Variable-Order Fractional Diffusion Model based Medical image denoising, Mathematical Problems in Engineering, Volume 2021 | Article ID 8050017 | https://doi.org/10.1155/2021/8050 017.
5. J.F. Aujol, G. Gilboa, T. Chan, and S. Osher, Structure-texture image decomposition modeling, algorithms and parameter selection,International Journal of Computer Vision, 67(1) (2006), 111–136.
6. J. Bai and X.C. Feng, Fractional-order anisotropic diffusion for image denoising, IEEE Transactions on Image Processing, 16(10) (2007), 2492–2502.
7. R. Campagna, S. Crisci, S. Cuomo, L. Marcellino and G. Toraldo, Modification of TV-ROF denoising model based on Split Bregman iterations, Applied Mathematics and Computation, 315 (2017), 453–467.
8. D. Chen, Y.Q. Chen and D. Xue, Fractional-order total variation image denoising based on proximity algorithm, Applied Mathematics and Computation, 257 (2015), 537–545.
9. Diana Andrushia, N. Anand and Prince Arulraj, Anisotropic diffusion based denoising on rete images and surface crack segmentation, International Journal of Structural Integrity, (2019), To print.
10. P. Guidotti and K. Longo, Two enhanced fourth order diffusion models for image denoising, Journal of Mathematical Imaging and Vision, 40(2) (2011), 188–198.
11. E. Isaacson and H.B. Keller, Analysis of Numerical Methods, Wiley, New York, 1966.
12. M. Lysaker, A. Lundervold and X.C. Tai, Noise removal using fourth order partial differential equations with applications to medical resonance images in space and time, IEEE Transactions on Image Processing, 12 (2003), 1579–1590.
13. Matheieu, P. Melchior, A.Oustaliup and C. Ayral, Fractional differentiation for edge detection, Signal Processing, 11 (2003) 2421–2432.
14. M. Nikolova, A variational approach to remove outliers and impulse noise, Journal of Mathematical Image Vision, 20(1-2) (2004) 99–120.
15. Y.F. Pu, P. Siarry, J.Zhou, Y.G. Liu, N.Zhang, G. Huang and Y.Z. Liu, Fractional partial differential equation denoising models for texture image, Science China Information Sciences, 57(7) (2014), 1–19.
16. Y.F. Pu, N. Zhang, Y. Zhang and J.L. Zhou, A texture image denoising approach based on fractional developmental mathematics, Journal of Pattern Analysis and Applications, 19(2) (2016), 427–445.
17. L.Rudin, S. Osher and E. Fatemi, Nonlinear total variation based noise removal algorithms, Physica. D, 60 (1992), 259–268.
18. H.R. Shahdoosti and O. Khayat, Combination of annisotropic diffusion and nonsubsampled shearlet transform for image denoising, Journal of Intelligent Fuzzy Systems, 30(6), (2016), 3087–3098.
19. G. Sudha Priya, P. Prakash, J.J. Nieto and Z. Kayar, Higher-order numerical scheme for fractional heat equation with Dirichlet and Neumann boundary condition, Numerical Heat Transfer, Part-B, 63 (2013), 540–559.
20. Tadjeran and M.M. Meerschaert, A second order accurate numerical approximation for the two-dimensional fractional diffusion equation, Journal of Computational Physics, 220 (2007), 813–823.
21. M.J. Wang and S.X. Deng, Image restoration model of PDE variation, IEEE Information and Computer Sciences, 2 (2009), 184–187.
22. J. Wu and C. Tang, PDE-based random valued impulse noise removal based on new class of controlling function, IEEE Transactions on Image Processing, 20(9) (2011), 2428–2438.
23. A.A. Yahya, J. Tan and M. Hu, A blending method based on partial differential equations for image denoising, International Journal of Multimedia Tools and Applications, 73(3) (2014), 1843–1862.
24. Y.L. You and M. Kavesh, Four-order partial differential equations for noise removal, IEEE

Transactions on Image Processing, 9(10) (2009), 1723–1730.
25. W. Zeng, X. Lu and X. Tan, A local structural adaptive partial differential equation for image denoising, International Journal of Multimedia Tools and Applications, 74(3) (2015), 743–757.
26. W. Zhang, J.Li and Y.Yang, Spatial fractional telegraph equation for image structure preserving denoising, Signal Processing, 107 (2015), 368–377.
27. J. Zhang, Z. Wei and L. Xiao, Adaptive fractional order multi-scale method for image denoising, Journal of Mathematical Imaging Vision, 43 (2012), 39–49.

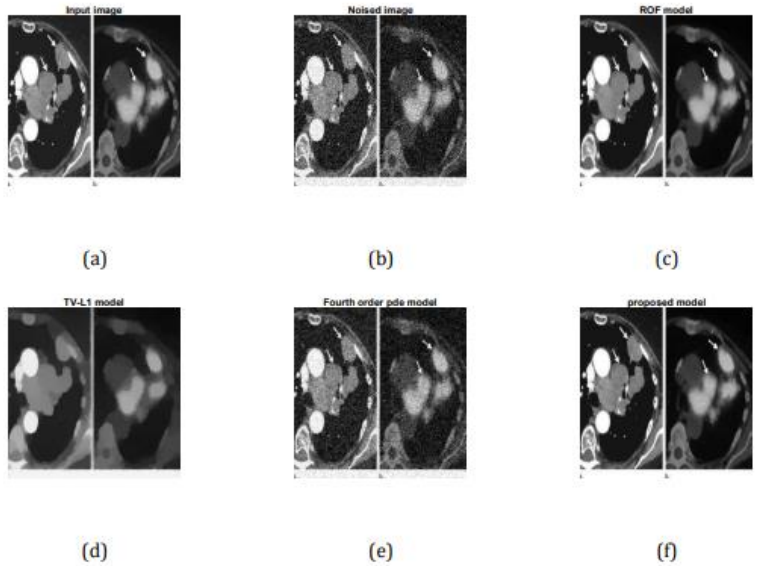

FIGURE 2: The denoising results of PET/CT-lung image

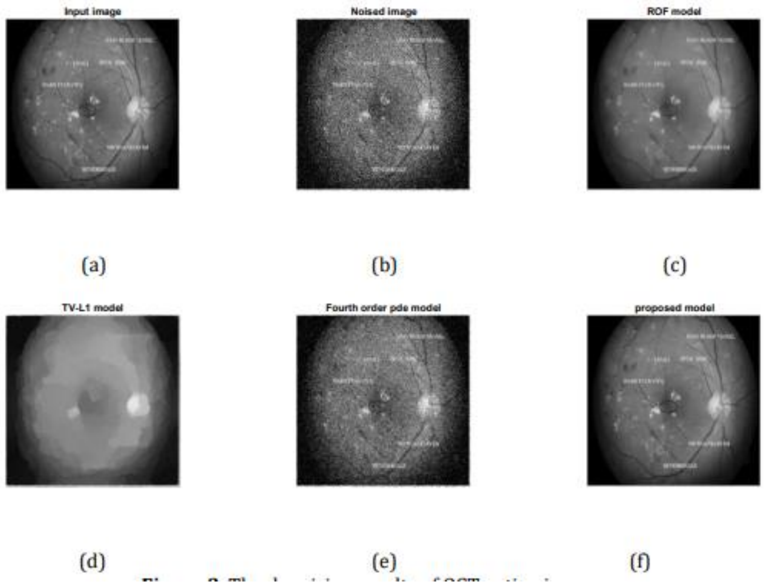

FIGURE 3: The denoising results of OCT-retina image

FIGURE 4: The denoising results of X-ray image

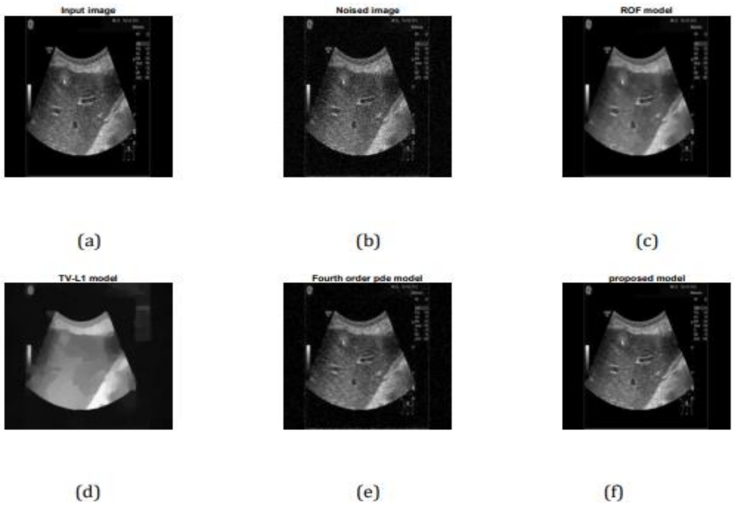

FIGURE 5: The denoising results of Ultra sound image

TABLE 1: Maximum absolute numerical

$\frac{1}{10}$	2.61×10^{-2}
$\frac{1}{20}$	2.11×10^{-2}
$\frac{1}{30}$	1.93×10^{-2}
$\frac{1}{50}$	9.86×10^{-3}
$\frac{1}{100}$	8.79×10^{-3}

Models	σ = 10	σ = 15	σ = 20	σ = 25	Average	CPU/Iterations(sec)
Image a: MRI-cervical spine image (λ=0.5882 and α = 1.6)						
ROF	30.48	30.37	30.12	29.84	30.20	0.331
$TV - L1$	36.76	36.68	36.36	36.09	36.47	0.446
Proposed	55.93	55.56	55.65	55.24	55.60	0.581
Fourth order pde	45.55	45.58	46.76	47.63	46.38	0.610
Image b: PET/CT-lung image (λ = 0.5617 and α = 1.6)						
ROF	28.46	28.16	27.98	27.52	28.03	0.187
$TV - L1$	29.44	29.48	29.18	28.89	29.25	0.856
Proposed	53.04	52.89	52.45	52.87	52.81	0.378
Fourth order pde	34.15	34.14	33.92	33.43	33.91	0.934
Image c: OCT-retina image (λ = 0.5699 and α = 1.6)						
ROF	29.76	26.64	26.22	25.98	27.15	0.219
$TV - L1$	32.56	32.44	32.23	32.02	32.31	0.740
Proposed	49.14	49.01	48.74	48.45	48.835	0.345
Fourth order pde	45.26	45.87	45.21	45.09	45.36	0.967
Image d: X-ray image (λ = 0.5843 and α = 1.6)						
ROF	29.97	29.15	29.68	28.46	29.32	0.467
$TV - L1$	32.78	32.15	32.12	31.87	32.23	0.421
Proposed	53.69	53.49	53.20	52.89	53.32	0.375
Fourth order pde	48.22	47.56	46.91	44.90	46.90	0.436
Image e: Ultra sound image (λ=0.5982 and α = 1.6)						
ROF	30.45	30.66	30.34	30.23	30.42	0.345
$TV - L1$	34.76	34.89	34.76	34.61	34.76	0.650
Proposed	54.12	53.56	53.65	52.98	53.58	0.561
Fourth order pde	44.87	44.58	44.75	43.89	44.52	0.615

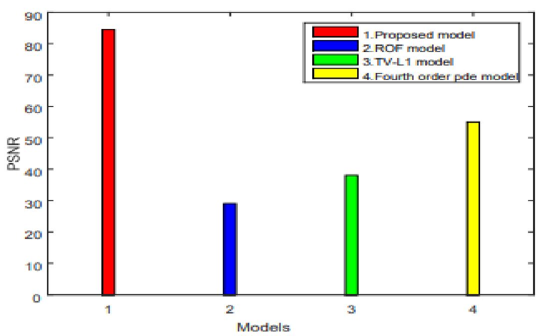

FIGURE 6: Comparison of PSNR values for four models in α ∈ [1,2]

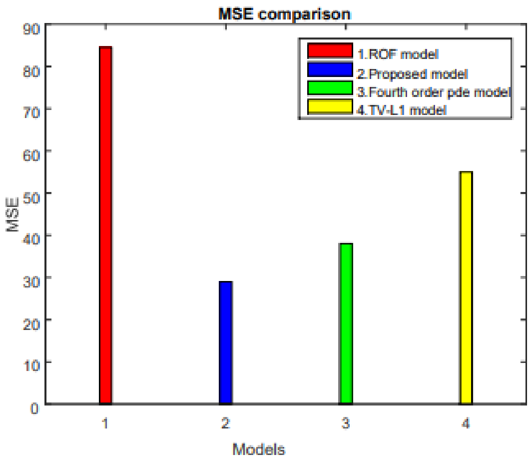

FIGURE 7: Comparison of MSE values for four models

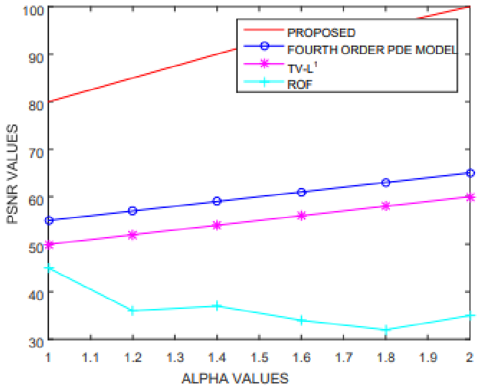

FIGURE 8: Comparison between PSNR values of four models